arXiv:1610.02227v1 [q-bio.NC] 7 Oct 2016

Geometric–optical illusions and Riemannian geometry

Werner Ehm[a] and Jiří Wackermann[b]

[a] Heidelberg Institute for Theoretical Studies, Schloss-Wolfsbrunnenweg 35, 69118 Heidelberg, Germany, werner.ehm@h-its.org

[b] Independent researcher, 79261 Gutach, Germany, mail@jiri-wackermann.eu

Abstract

Geometric-optical illusions (GOI) are a subclass of a vast variety of visual illusions. A special class of GOIs originates from the superposition of a simple geometric figure ("target") with an array of non-intersecting curvilinear elements ("context") that elicits a perceptual distortion of the target element. Here we specifically deal with the case of circular targets. Starting from the fact that (half)circles are geodesics in a model of hyperbolic geometry, we conceive of the deformations of the target as resulting from a context-induced perturbation of that "base" geometry. We present computational methods for predicting distorted shapes of the target in different contexts, and we report the results of a psychophysical pilot experiment with eight subjects and four contexts to test the predictions. Finally, we propose a common scheme for modeling GOIs associated with more general types of target curves, subsuming those studied previously.

Keywords: calculus of variations, Ehrenstein–Orbison type illusions, geodesic, geometric–optical illusions, Poincaré model, Riemannian geometry, vector field, visual perception

Abbreviations: GOI: geometric–optical illusion, LI: local interactions, PDF: Portable Document Format, PM: Poincaré model, RO: regression to orthogonality, VHI: vertical–horizontal illusion

1 Introduction

Visual perception informs us about the outward reality in the surrounding space. Under certain circumstances, the result of a perceptual process ("percept", for short) may remarkably differ from our knowledge of the objective reality as it is evidenced, e. g., by measurement results, cognitive inferences, or other percepts. Those situations are commonly known as "visual illusions."[1] Visual illusions are not deliberate deceptions or random errors of the visual system; they are systematically occurring, experimentally reproducible and measurable phenomena, presumably revealing essential properties of the visual system, and as such they are a proper subject of scientific study (Metzger,

[1] Of course, perceptual illusions are known also in other sensory modalities, or occurring as intermodal interactions. However, these types of illusions are not in our focus, nor are visual illusions affecting optical qualities such as brightness or color, and phenomena involving illusory motion. An exhaustive overview of the field is beyond the scope of the present paper.

1975; Coren and Girgus, 1978; Robinson, 1998; Eagleman, 2001). Following Gregory's (1997b) proposal, visual illusions can be roughly subdivided into four types: fictions, paradoxes, ambiguities, and distortions.

Geometric–optical illusions (GOI) are an interesting subclass of visual *distortions*. In GOIs, geometric properties of a stimulus—e. g., lengths, angles, areas, or forms—are affected and systematically altered by the presence of other elements in the visual field. For example, a straight line appears slightly curved when superposed with an array of straight or curved lines (Hering, 1861); a length marked by two distinct elements appears larger if the space between them is subdivided by additional elements (Oppel, 1861; Kundt, 1863); two equally long line segments appear different when marked by arrows of opposite orientation (Müller-Lyer, 1889, probably the most popular GOI); etc. These phenomena were discovered and named about one and a half century ago (Oppel, 1855), and since then their number significantly expanded. Despite numerous classificatory (Coren et al., 1976; Gregory, 1997b) and explanatory attempts (Changizi et al., 2008; Coren and Girgus, 1978) based on optical, retinal, cortical or cognitive mechanisms, there is by now no unitary theory of GOIs, let alone of visual illusions on the whole. There is not even consensus about general principles upon which such a theory could or should be based (Wackermann, 2010; Zavagno, Daneyko, and Actis-Grosso, 2015). Nonetheless, the GOIs deserve special attention: not only because, historically, they "form the core of the subject [of visual illusions]" (Robinson, 1998, p. 11), but also for their link to geometry-based theories of visual perception.

In the present paper we aim at a *phenomenological* theory of GOIs; that is, we search for a mathematical representation of the phenomena under study, not for an explanation via physiological or psychological mechanisms. Our focus is on a special class of GOIs based on interactions between a *target* element and *context* elements in the visual field. In our previous work (Ehm and Wackermann, 2012) we were studying Hering type illusions, where the target was a segment of a straight line. Here we consider the case where the target is a *circle*, such as in Figs. 1a, 1b. These and similar illusions were described, independently and in different conceptual frameworks, by Ehrenstein (1925) and Orbison (1939). Illusions of this type and of Hering type have in common the *angular expansion* effect, also known as "regression to right angles" (Hotopf and Ollerearnshaw, 1972; Hotopf and Robertson, 1975): the illusory distortion of the target acts so as to enlarge the acute angles at the intersection points. It is thus plausible to assume that a common approach may account for both groups of phenomena.

In our earlier paper (Ehm and Wackermann, 2012) we modeled the distorted percepts of a straight line segment (target) by the solutions of a variational problem, namely as the shortest path connecting the endpoints of the target when length is measured in terms of a context-induced perturbation of the Euclidean metric. In regard to the circular targets in Ehrenstein–Orbison type illusions the questions arise: can this principle be

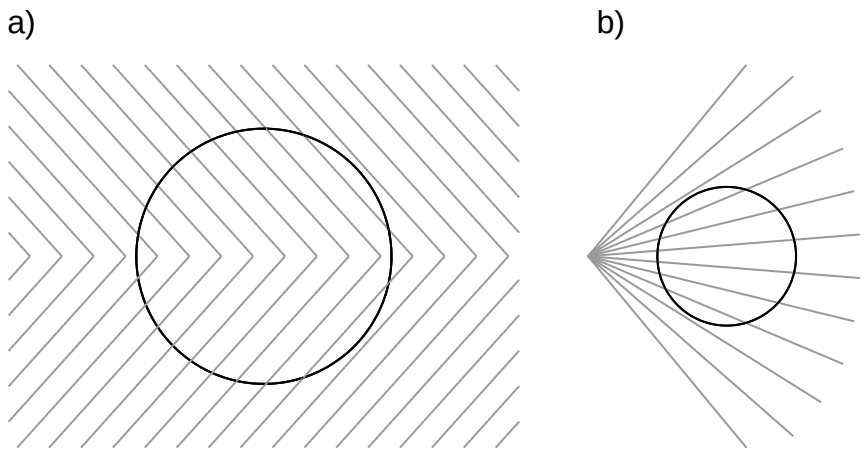

Figure 1. Two examples of GOIs with a circular target, adapted from Orbison (1939) and Ehrenstein (1925). Although the targets are perfect circles, they appear to the observer as being slightly inward-dented on the right-hand side (a) or on the left-hand side (b).

generalized? And, if so, how to overcome the restriction to straight-line targets inherent in the original approach? The basic idea permitting an extension to curved targets consists in *equipping the target itself with a geometry* (Ehm and Wackermann, 2013). In this view both the target and the distorted percepts figure as paths of shortest length (geodesics) in an appropriate "base" geometry and a context-induced perturbation of that geometry, respectively. In the present paper we elaborate on this approach, using the fact that half circles represent geodesics in a suitable model of hyperbolic geometry.

The elements of this framework are presented in Section 2. We introduce the base and the perturbed hyperbolic geometries and describe the single steps leading to our final prediction of the distorted percept. The details are deferred to the mathematical appendices. An experiment intended to verify the predictions and to measure the magnitude of the illusory distortion is reported in Section 3. The discussion in the final Section 4 addresses phenomenological as well as modeling aspects. It concludes with the above indicated proposal for a general approach covering GOIs of the Hering and the Ehrenstein–Orbison type as special cases.

2 Mathematical model

2.1 Preliminary remarks

Our mathematical description of the visual distortion of the target figure draws on minimum principles related to geometrical conceptions. We think of the context figure

as distorting the spatial relationships between the points of the drawing plane, similar to when an elastic substance is kneaded: some portions are expanded while others are condensed. Riemannian geometry (Laugwitz, 1965) makes it possible to describe such situations mathematically by means of a locally varying metric that attaches a well-defined length to every path through the respective range. The connection to minimum principles comes via the concept of a *geodesic,* which is a path of minimal length, measured in the respective metric, that connects two given points. In fact, geodesics also represent paths requiring minimum energy or effort, rendering them relevant to fundamental conceptions about human perception; cf. Section 4.3.

According to our basic surmise the percept of the circular target can be modeled as a geodesic in a suitable geometry that is perturbed by the context if such is present. It is known that a (2D) Riemannian geometry admitting only circles and straight lines as geodesics must have constant curvature (Khovanskii, 1980). The possible candidates for a "suitable" or *base* geometry thus must be one of the classical elliptic, Euclidean, and hyperbolic geometries. Among these only Poincaré's half plane model of hyperbolic geometry [PM] fulfills the following three conditions essential to our approach.[2]

i) The base geometry has to have circle segments as geodesics—so does the PM.

ii) The perceptual distortions are hypothesized to obey the local interactions principle, particulary, to depend on the intersection angles between the context and the target lines. Therefore, the intersection angles should be represented faithfully—the PM is conformal.

iii) The relevance of geometries derived from immersions of a surface into $\mathbb{R}^3$ appears doubtful considering that our stimulus figures are presented, and seen, on a flat screen—the PM implements the distortions of the Euclidean metric entirely within (a subset of) $\mathbb{R}^2$.

To summarize, adopting the PM for the base geometry is virtually cogent for our modeling approach. The PM allows us to deal with circular targets essentially along the same lines as with the straight line targets considered in the earlier work (2012), although the details are rather more involved. In this section we only present the main lines of our geometrical approach; the mathematical elaboration is postponed to the appendices.

[2]Strictly speaking, Poincaré's disc model (Cannon et al., 1997) satifies (i) to (iii), too. However, it serves our purposes less well as the geodesics span less than a half circle, and the contexts have to be placed in the disc; both circumstances imply substantial restrictions.

2.2 Poincaré model of the hyperbolic plane

The Poincaré model equips the upper half plane $\mathcal{H} = \{\xi = (\xi_1, \xi_2) \in \mathbb{R}^2,\, \xi_2 > 0\}$ with the line element $ds^2 = (d\xi_1^2 + d\xi_2^2)/\xi_2^2$. (For comparison, the Euclidean line element is $d\xi_1^2 + d\xi_2^2$.) This means that the length of a smooth curve $t \mapsto x(t) = (x_1(t), x_2(t))$, $t_0 \le t \le t_1$ in $\mathcal{H}$ is, invariantly under reparameterization, defined as

$$L(x) = \int_{t_0}^{t_1} \frac{|\dot{x}(t)|}{x_2(t)}\, dt = \int_{t_0}^{t_1} \sqrt{\langle \dot{x}(t), H(x(t))\, \dot{x}(t)\rangle}\, dt. \tag{1}$$

Here $\dot{x}$ stands for $dx/dt = (dx_1/dt, dx_2/dt)$, and $|\cdot|$ and $\langle\cdot,\cdot\rangle$ denote the standard Euclidean norm and inner product, respectively. In the last term of (1),

$$H(\xi) = \xi_2^{-2} I \quad (\xi \in \mathcal{H}) \qquad \text{where} \qquad I = \begin{pmatrix} 1 & 0 \\ 0 & 1 \end{pmatrix}. \tag{2}$$

The matrices $H(\xi)$ give rise to the metric tensor of the Riemannian geometry associated with the Poincaré model. Since they are scalar multiples of the identity matrix I it is evident that angles are preserved in this geometry, that is, they are identical with the Euclidean angles. Lengths, however, are not preserved, and geodesics need not be "straight" in the usual sense. In fact, all geodesics in the hyperbolic plane are segments of the following two types of curves: (a) vertical lines in $\mathcal{H}$ (parallel to the x_2 axis); (b) half circles in $\mathcal{H}$ orthogonal to the x_1 axis (satisfying $(x_1 - a)^2 + x_2^2 = r^2$ for some $a \in \mathbb{R}$, $r > 0$); see Fig. 2.

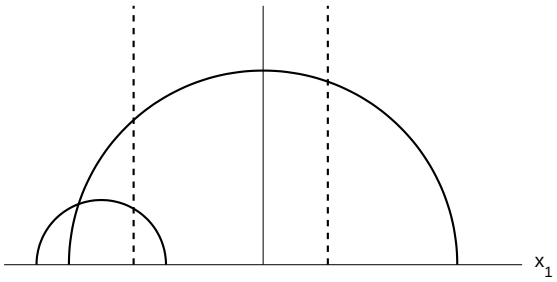

Figure 2. Geodesics in the Poincaré model: half circles and straight lines orthogonal to the x_1 axis.

2.3 Target, context, and the perturbed hyperbolic geometry

Circles with center at the origin will serve as the target component of our stimulus figures. The context component is represented by means of a smooth planar vector field of unit directions $v(\xi)$ ($|v(\xi)| = 1$, $\xi \in \Xi$; v twice continuously differentiable) defined on a region Ξ that contains the target. A finite sample of the stream lines of v makes up the context curves actually presented to the observer.

The Poincaré model requires decomposing the complete figure into the two parts contained in the upper and the lower half planes, respectively. These two parts will be treated separately. At first, we consider the upper part, and (segments of) upper half circles as targets. Given a parameter $\alpha \geq 0$ that accounts for the strength of the distortion, the context-pertubed Riemannian geometry in the upper half plane is determined by declaring the length of a curve x in $\mathcal{H}$ as

$$L_\alpha(x) = \int_{t_0}^{t_1} \sqrt{\langle \dot{x}(t), H_\alpha(x(t))\, \dot{x}(t) \rangle}\, dt, \tag{3}$$

with positive definite matrices

$$H_\alpha(\xi) = \xi_2^{-2} G_\alpha(\xi) \quad \text{where} \quad G_\alpha(\xi) = I + 2\alpha\, v(\xi) \otimes v(\xi) \qquad (\xi \in \Xi \cap \mathcal{H}). \tag{4}$$

This definition implements two basic principles already employed by Ehm and Wackermann (2012):

(a) the *local interactions* [LI] hypothesis: the context v "acts" only along the candidate curves, in the vicinity of the target;

(b) the *regression to orthogonality* [RO] hypothesis: the distortion operates toward an expansion of the acute angles at the points of intersection.

Both these hypotheses, supported by experimental phenomenology (cf. Horrell, 1971; Wackermann, 2010), are built into the expression for the curve length $L_\alpha(x)$, which when evaluated explicitly becomes

$$L_\alpha(x) = \int_{t_0}^{t_1} \frac{\sqrt{|\dot{x}(t)|^2 + 2\alpha \langle \dot{x}(t), v(x(t)) \rangle^2}}{x_2(t)}\, dt. \tag{5}$$

By (5), the context vector field enters $L_\alpha(x)$ only locally at the curve x [LI]; and the term $\langle \dot{x}(t), v(x(t)) \rangle^2$ penalizes non-orthogonality (for positive α) between the vector field v and the tangents of x [RO]. A geodesic thus realizes an optimal compromise between being *as short as possible*, and passing through the stream lines of v *as orthogonally as possible*. We denote the H_α geodesic with the same endpoints as the target as γ_α. It represents our ideal candidate for the prediction of the actual, distorted percept of the target stimulus. A necessary condition for a curve x to be a geodesic in the H_α metric is given in the form of a second-order nonlinear differential equation (Appendix A, Proposition 1).

2.4 "Prediction" of the distorted percept, and shape of the distortion

The exact geodesic γ_α is not known explicitly, and we have to rely on approximations to this first candidate for the prediction of the distorted percept. Here we outline the

main steps leading to our final prediction, thereby leaving out the mathematical details in order to simplify the presentation. Those details are fully treated in the appendices B, C, and D.

For definiteness, let the vector field v be fixed, and let τ denote the target half circle which is supposed to be of radius $r > 0$, with center at the origin.

Shape of the distortion. For $\alpha = 0$ the target half circle τ is an exact geodesic in the $H_0 \equiv H$ metric, namely $\tau = \gamma_0$. Since the visual distortion is expected to be small, though discernible, the effect magnitude α, and likewise, the deflection of the geodesic γ_α from τ, should be small, too. Therefore, it is plausible to try an *ansatz*

$$\widehat{\tau} \doteq \tau + \alpha\sigma =: \widetilde{\tau}$$

for the prediction $\widehat{\tau}$ of the distorted percept, with σ arising as the limit of $(\gamma_\alpha - \tau)/\alpha$ as $\alpha \to 0$. As such, σ only depends on v and τ, not on α; hence we call σ the (approximate) *shape* of the deflection. It is determined by another differential equation similar to the one characterizing γ_α (Appendix C, Proposition 2).

Adding the lower part. Thus far, we only considered the part of the stimulus figure lying in the upper half plane and described the (preliminary) prediction $\widetilde{\tau} \equiv \widetilde{\tau}_+$ for the percept of the upper half of the target circle. This is sufficient if the figure is symmetrical about the x_1 axis. Otherwise we proceed as follows: the lower part is mirrored at the x_1 axis into the upper half plane and is processed there in the same way as the upper part; after modification, it is mirrored back to the lower half plane, yielding the prediction $\widetilde{\tau}_-$ for the percept of the lower part of the target circle. By construction, the two parts meet at their endpoints and together give the preliminary prediction $\widetilde{\tau} = \widetilde{\tau}_- \cup \widetilde{\tau}_+$ for the full target circle.

Area conservation. We can now state the *final form,* for given parameter α, *of our "prediction"* $\widehat{\tau} \equiv \widehat{\tau}_\alpha$ for the distorted percept of the full target circle:

$$\widehat{\tau} = \kappa\, \widetilde{\tau}$$

where the scale factor $\kappa \equiv \kappa_\alpha > 0$ is chosen such that the area enclosed by the curve $\widehat{\tau}$ equals $r^2\pi$, the area of the target circle. The purpose of this renormalization is to adjust for potential size effects that have nothing to do with the perceptual distortion induced by the context. The quotation marks in "prediction" shall once more emphasize the circumstance that our approach yields a proper prediction only for the shape of the distortion; the parameter α measuring its strength yet has to be determined experimentally.

3 Experimental demonstration

The purpose of the reported pilot experiment was (a) to verify qualitatively the prediction of the context-induced distortion shape following from our model, and (b) to assess quantitatively the magnitude of the distortion effect as measured by the parameter α. According to the regression to orthogonality hypothesis RO, α should be nonnegative, so that a prevalence of positive estimates $\widehat{\alpha}$ can be seen as empirical support for RO. One may expect that α actually depends on a number of factors such as context, participant, specific experimental conditions, etc. A study of such systematic variations is beyond the present scope, however, and we will focus on the sign of the $\widehat{\alpha}$s only.

For the experimental determination we employed again the method of *compensatory measurement*, where the magnitude of the "counter-distortion" for which the perceptual distortion vanishes serves as a measure of the real distortion. The rationale is obvious: if τ is perceived as $\tau + \alpha\,\sigma$, then (for small α) $\tau - \alpha\,\sigma$ will approximately be perceived as τ (cf. Ehm and Wackermann, 2012, p. 409).[3] The procedure based thereupon is obvious as well: a series of circular targets distorted in the opposite direction is presented to the observer, who adjusts α until s/he perceives a perfect circle.

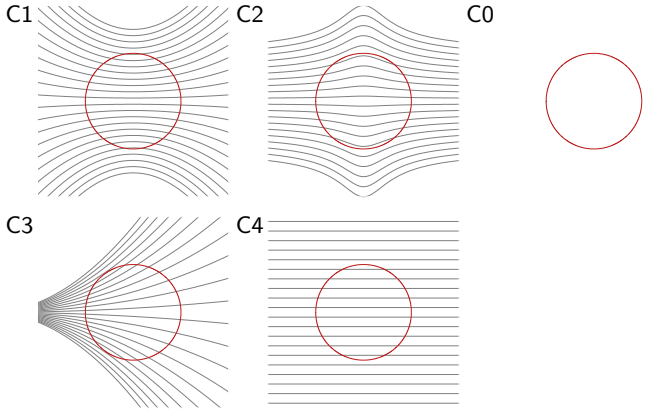

Figure 3. Stimuli used in the experiment. Red closed curves are *exact* circles ($\alpha = 0$), superposed on context patterns (grey, C1–C4) or on a blank background (C0).

The stimuli were constructed for four different contexts C1 to C4, as shown in Fig. 3 and specified in Appendix E. For each context, a series of 31 pictures was generated, showing the same array of context curves superposed with differently deformed targets of the form $\widehat{\tau}_{\alpha_k} = \tau - \alpha_k\,\sigma$, $(k = 1, \ldots, 31)$, with coefficients α_k varied in a sufficiently large range. As a no-context control condition (C0), another stimulus series was constructed consisting of 31 pictures of ellipses on a blank background, with the main axes aligned

[3] This method has a long tradition in the GOI research: Zöllner was probably the first to use it for the measurement of the context-induced tilt of straight lines, another GOI now named by him (Zöllner, 1860, 1872). For another use of this method (dubbed "nulling paradigm") in a dynamical, motion induced visual illusion cf. Yazdanbakhsh and Gori (2011).

with the horizontal and vertical axis, respectively, and half-axes ratios r_2/r_1 varied as $1 + \alpha_k$ while keeping the area constant across the picture series. This condition was included to check for a possibly confounding effect of the "vertical–horizontal illusion" (VHI) as explained in Section 4.1. Details regarding the preparation of the stimuli and the experimental design are given in the supplementary online material.

Eight observers participated in the experiment. The contexts C1 to C4 were shown either in their original orientation (symmetry axis horizontal) or rotated by 90°, with two repetitions each. Interspersed were five control trials using the no-context stimuli C0, summing up to 21 stimulus presentations in a single session. We thus obtained a total of 168 parameter estimates $\widehat{\alpha}$. The complete set of estimates $\widehat{\alpha}$ is presented in Fig. 4.[4] Evidently, the average $\widehat{\alpha}$s for each pair of a subject and a (genuine) context are positive, with one single exception among the 32 cases (4 contexts × 8 subjects). This indicates that, statistically, the direction of the perceptual distortion is correctly predicted by our approach. That not all α estimates are positive, as it was the case in our earlier study of straight line targets (Ehm and Wackermann, 2012), is of little surprise given the small effect magnitude on the one hand, and the considerable intra-individual variance of the responses on the other hand.

As for the possible influence of the VHI (see Section 4.1), there is little evidence for a systematic overestimation of vertical extents: in the control condition C0, 5 out of 8 of the average $\widehat{\alpha}$s are positive (fraction of single trial positive $\widehat{\alpha} = 0.625$, corresponding to $p \approx 0.08$, one-sided sign test). For the contexts C1 to C4 the tendency for positive α estimates is significantly higher (31 out of 32 of the average $\widehat{\alpha}$s are positive; fraction of single trial positive $\widehat{\alpha} = 0.766$, corresponding to $p < 10^{-9}$, one-sided sign test). It is thus unlikely that the results of the experiment could be reduced to a vertical vs. horizontal bias.[5]

4 Discussion

The similarities and differences of our geometric modeling approach with the related work of Hoffman (1966, 1971), Smith (1978), and Zhang and Wu (1990) were already expounded in our earlier communication (Ehm and Wackermann, 2012). Here we will

[4] The results for the control C0 are displayed together with those for the contexts C1 to C4 only for parsimony of presentation; a direct, quantitative comparison of the estimates across the conditions is not meaningful.

[5] The case of the context C4, consisting of parallel horizontal lines, deserves an extra comment. As indicated by average $\widehat{\alpha} > 0$, the target subjectively appeared larger in the vertical than in the horizontal extension, which—as just argued—was not due to a vertical vs. horizontal bias. This finding seems to be in agreement with the "filled space expansion," special cases of which are the Oppel–Kundt illusion or Helmholtz squares (Robinson, 1998; Wackermann, 2011b). On the other hand, the perceived vertical elongation is in striking contrast with the familiar dressmaker's wisdom: to appear slim avoid wearing clothes with horizontal stripes (cf. also Thompson and Mikellidou, 2011).

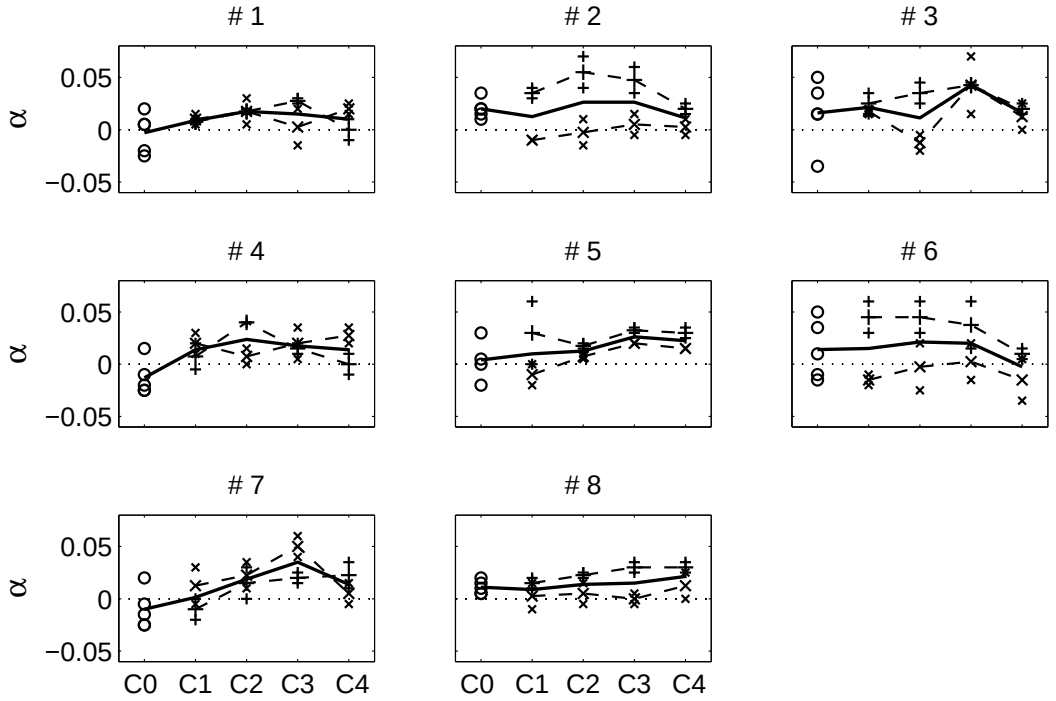

Figure 4. Results of the experiment. For each subject, the single-trial α estimates are plotted vs. control condition C0 and context patterns C1 to C4. Different markers are used for C0 ('$\circ$') and the contexts C1 to C4 ('$\times$'). The average of the single trial $\widehat{\alpha}$s is marked by a diamond for condition C0, and by a solid line for the others.

focus on several other issues of interest that were not, or only marginally, addressed therein.

4.1 Problem of "phenomenal correctness"

The modeling approach outlined in Section 2 yields, for a given context, a prediction for the shape of the distorted circular target. Obviously, we cannot exclude the existence of alternative shapes yielding a still better perceptual fit to a perfect circle. Naturally then, the question arises how to assess the merit of our prediction? It should be clear that a fully satisfactory answer is out of reach, on the following grounds.

In contrast with some other GOIs in which only one parameter of the stimulus is affected (e. g. length of a line segment, as in the Müller-Lyer illusion), the space of possible deformations of a circle into ovals and other closed curves is of infinite dimension. As it is thus impossible to exhaust all possible deformations, only a limited selection of

(counter-)distortions could be presented to the observers for a comparative judgment. This requires, on the one hand, suitable theories or models delivering meaningful candidates for such a selection, that ought to incorporate the variation of the perceptual distortions with the context. Here our approach could be most helpful, as it specifies a concrete context-specific shape of the distortion. On the other hand, the sheer difficulty of having to distinguish between very similar oval-shaped forms sets substantial limitations to experimental approaches. As attested by the variability in our α estimates, such a task presents a serious challenge to the observers' perceptual faculties even when, as here, the shape is fixed and only one parameter (magnitude) is to be adjusted.

One may wonder whether, at least with sufficiently symmetrical contexts, a simple comparison between the figure's extent along its horizontal and vertical axes might also provide a convenient cue as to a deviation from circularity. It is known since the very beginnings of GOI research (Oppel, 1855) that linear extents in the vertical direction are overestimated relatively to the horizontal direction (Robinson, 1998, p. 96–100). This so-called "vertical–horizontal illusion" (VHI) is usually demonstrated in T-shaped or L-shaped line-drawn figures (Lehmann, 1967; Avery and Day, 1969; Robinson, 1998; Wolfe, Maloney, and Tam, 2005), but it can also be observed in the perception of two-dimensional forms or three-dimensional real-world objects (Metzger, 1975). This was the rationale for including the control condition in our experiment, in order to evaluate the observers' ability to distinguish between circular and ellipsoidal forms, unaffected by a context. In fact, a VHI effect could easily be incorporated in our model by replacing

$$I = \begin{pmatrix} 1 & 0 \\ 0 & 1 \end{pmatrix} \to \begin{pmatrix} 1 & 0 \\ 0 & \beta^2 \end{pmatrix} \qquad \text{for some } \beta > 0$$

in the definition of the metric tensors (cf. (2), (4)). However, our experimental data provided little if any evidence for a significant VHI influence (Section 3). It is thus doubtful that the flexibility gained by an additional parameter, β, would compensate for the further increased difficulty of the perceptual task.

Notwithstanding the difficulties, we can say that our approach yields predictions capturing essential features of the observed distortions. The experimental data (prevalence of positive α estimates) and direct observation corroborate this claim (cf. Fig. 5).

4.2 Geometry of visual space

Our geometric paradigm may be reminiscent of studies of the metric properties of visual space, a topic at times intensely debated in the vision research. The hypothesis of a non-Euclidean structure of visual space, introduced by Luneburg (1948, 1950), elicited a respectable amount of theoretical (Suppes, 1977; French, 1987) and experimental work (for reviews see Indow, 1991; Wagner, 2006; Westheimer, 2008). Those studies, however, were concerned with the geometry of the "full" three-dimensional [3D] visual space,

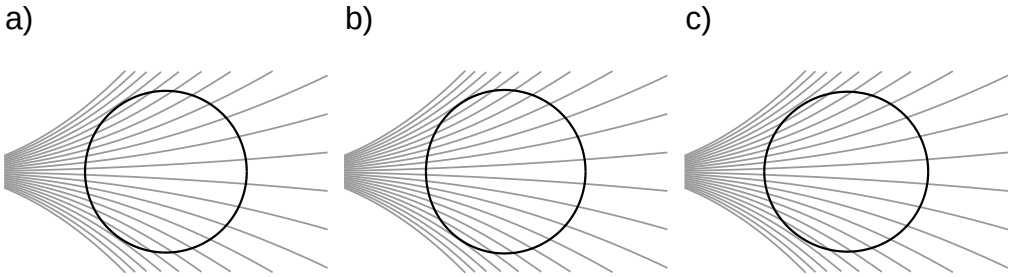

Figure 5. Regarding the "phenomenal correctness" of the model-based prediction. Context C3 with predictions $\widehat{\tau}_\alpha = \tau + \alpha\,\sigma$ for $\alpha = 0$ (a: perfect circle), $\alpha = +0.03$ (b: the indenting of the target at the left-hand side is strengthened w. r. t. the "pure illusion" in case a), and $\alpha = -0.03$ (c: counterbalancing yields an apparently circular shape).

as exemplified by Blumenfeld's (1913) experiments with the reproduction of visually assessed spatial distances. Also, in attempts of explaining some GOIs on the basis of a non-Euclidean geometry of visual space, differences between judgments in the "near" and "far" spaces play a rôle (Heelan, 1983). In fact, studies of "the" geometry of visual space remained remarkably inconclusive (Wagner, 2006), or at least they did not support the original hypothesis of a visual space described by a Riemannian geometry of constant curvature: "Instead, the geometry of visual space itself appears to be a function of stimulus conditions" (Wagner, 1985, p. 493). Again, this assertion may be remotely reminiscent of our own approach; however, there are substantial differences.

Firstly, the stimuli in our experiment are definitely 2D, a possible 3D interpretation notwithstanding. Hence, the present work is dealing with the perceived content of the visual *field*, understood as a 2D manifold of primary visual experience (Wackermann, 2011a).[6] Secondly, and most importantly, the geometry here is implicit, as it were, in the geometrical form of the *target* (e. g., Euclidean for straight lines, hyperbolic for circles). Aspects of vision and perception enter only via the *distortion* of that "base" geometry induced by *additional elements* (besides the target stimulus) in the visual field, namely, the context curves. Consequently, although the GOI phenomena are undoubtedly intertwined with the issues of visual space perception (Westheimer, 2008), there is no direct connection between our approach and the research into "the" geometry of visual space in general.

[6]Of course, the visual field can be conceived of as a basis upon which the "full" visual space is constituted. This, however, is a very complex issue involving not only facts of vision but also integration of optic, haptic, and kinesthetic data; that is, a topic definitely beyond the scope of the present work.

4.3 Explanatory status of the present theory

The approach taken in the present and the earlier (Ehm and Wackermann, 2012) study is expressly "phenomenological," that is, we are not aiming at explanations via the underlying neural or psychological mechanisms. This is a legitimate choice, adopted by other authors in the field as well (e. g. Hoffman, 1966; Smith, 1978; Wagner, 1985). Notwithstanding this confinement, our approach does contain elements contributing to a better understanding of the GOIs under study.

The visual field, as well as the respective retinal or cortical areas, are 2D varieties. Our two principal assumptions, "local interactions" and "regression to orthogonality" (Section 2.3), would correspond to inhibitory lateral interactions between adjacent, orientation-specific elements (Burns and Pritchard, 1971; Carpenter and Blakemore, 1973). They thus furnish a clue for connections with the neurophysiology-based approach. However, unlike neural models proposed by other authors (e. g. Walker, 1973; Fermüller and Malm, 2004), our approach models the GOI phenomena where they occur, "out there" in the visual field, not in the retina or cortical areas.

This is not to say that the present approach does nothing for explanations of the GOIs. We only have to avoid the "mechanistic fallacy," where the explanation of a phenomenon is identified with its reduction to the mechanisms acting at the most fundamental level, and other kinds of theories are dismissed as "merely descriptive."[7] For example, Snell's law of refraction describing the path of light propagation in heterogeneous media is definitely a phenomenological law. As such, it is well able to explain large varieties of optical phenomena. But even more importantly, Snell's law and other facts of dioptrics and catoptrics can be subsumed under (or derived from) a single superordinated extremal principle, the Fermat's principle of least time. Explanations from such principles are not less "causal" than mechanistic explanations, but they rely upon a different notion of causality, namely that of the formal rather than the efficient cause.

The relevance of extremal principles for human perception was first pointed out by Ernst Mach (1866) who raised the question, "why a straight retinal image is seen [in the outward space] also as straight." In a more general note, he further speculated:

> "As is well-known, mechanics leads everywhere to [solving] minimization or maximization tasks. However, the importance of such minimal principles exceeds by far the special assumptions of mechanics. They occur everywhere where a multitude

[7] A clarification may be appropriate at this point. It is true that in the natural sciences the knowledge of "mechanisms"—i. e., of the elementary constituents of a system and of the rules governing their interactions—is the desirable and ultimate goal. This, however, does not imply that the whole of the scientific discipline is stated in terms of those elementary mechanisms. Descriptions of phenomena in purely functional terms abstracting from the elementary level lead to working theories as well. Disciplines such as thermodynamics, chemical kinetics, etc., operate without direct reference to the microscopic structure of matter or to elementary interactions between the individual molecules or atoms.

> [of elements] acts collectively, partly by facilitation, partly by inhibition. Also the eye, in seeing forms, is ruled by such principles." (Mach, 1868, p. 19)

Our study thus can be seen as a variation on this general theme (cf. also Hatfield and Epstein, 1985): to identify an overarching extremal principle from which special instances of "seeing the straight as straight"—or more generally, "seeing the shortest as shortest (in a given disturbed geometry)"—can be derived. We may speculate that this principle can be expressed in terms of "minimal energy" or "minimal effort": under static conditions as in the GOIs studied here, the visual system would relax to a kind of equilibrium state requiring the least effort needed to resolve a "perceptual tension" between the target figure and the context pattern. If a related macroscopic variable characterizing a given percept can be defined, it should find a counter-part in a model of the neural substrate on the mesoscopic or microscopic level. Our focus on a phenomenological theory thus does not preclude a connection to "mechanistic" models of GOIs: the present study may open a way for a research program integrating two different levels of modeling and theory.

To be sure, the question of how the visual system deals with motion or the uncertainties of 3D vision is highly relevant biologically, and experiments involving such elements help to better understand a number of visual illusions in terms of the links to and the working of the neural substrate; see e. g. Yazdanbakhsh and Gori (2011), Gori and Stubbs (2014). Conversely, such knowledge can lead to important insights, concerning e. g. the perceived integrity of an object under rigid motion (Zhang and Wu, 1990). Again, it cannot be denied that the existing explanatory theories of GOIs, specifically, lack consensus even about the most basic issues. Common explanations usually refer *either* to hypothetical cognitive processes *or* to physiological mechanisms (see e. g. Coren and Girgus, 1978). This duality reflects the principal controversy between "empiricist" and "nativist" approches to perception (cf. Boring, 1942; Turner, 1994), and continues up to the present (see e. g. Rogers, 2014; Maniatis, 2015). The neurophysiology approach searches the basis of GOIs and related phenomena in the intrinsic properties of the visual system (Livingstone and Hubel, 1987; Eagleman, 2001). Cognitive theories, by contrast, attempted to explain the GOIs via "unconscious inferences" (Helmholtz, 1867; Rock, 1977; Gregory, 1997a) based on additional hypotheses such as 3D interpretations of pictorial stimuli, as for example in Gregory's (1963) theory of "inappropriate constancy scaling". As for the 3D interpretation of GOI stimuli: there is no evidence that a planar drawing is *necessarily* seen as a 3D scene (Wackermann, 2011a). The same can be said about other hypothetical constituents of those theories, such as "imagined motions" (Ehrenstein, 1925; Changizi et al., 2008). No doubt, there *are* phenomena involving 3D vision as well as illusory or real motion (see e. g. Yazdanbakhsh and Gori, 2011). However, the specific character of the GOIs under study, which occur in the 2D visual field and are purely static in nature, furnishes no evidence, at this point, how

those elements could be incorporated in our approach.

4.4 Conclusion and outlook

The present work extends our earlier work about geometric–optical illusions (Ehm and Wackermann, 2012) from straight line targets to circle targets. Thereby we had to overcome some technical difficulties: since the geodesics in the appropriate (hyperbolic) geometry are *half* circles, we had to divide the stimulus in two parts and to recombine the distorted percepts. Another, rather technical issue concerned the problem of aligning the distorted percept to the target (Appendix B). A certain degree of arbitrariness is always involved. However, the influence of those arbitrary choices appears to be immaterial. E. g., rotating the stimulus by 90° has but a minor effect on the predicted percept while the major qualitative features of the distortion are maintained. Also, bisecting the stimulus along the x_1 axis is not unnatural as the horizontal axis *has* an outstanding direction, considering the position of the eyes (which were fixated during the experiment). Finally, in accordance with the "local interactions" hypothesis the illusory distortion is observable not only in full circles, but also when using circular *arcs* as targets.

The initial motive for the present work was to explore the scope of the geometrical approach adopted in our earlier paper on straight line targets. We found that the case of a circle target could be reconciled with the former framework by conceiving of the target itself as a geodesic in a suitable base geometry. The apparent commonalities of the two special cases lead us to propose the following general approach to the modeling of geometric–optical illusions of the "target–context" type (cf. Fig. 6):

Consider (only) targets that are geodesics in some base Riemannian geometry associated with metric tensor M; model the illusory percept of the target as a geodesic in another geometry associated with a (small) context-dependent perturbation $\widetilde{M}$ of M (which involves the "local interactions" and "regression to right angles" principles).

Applications of this framework to other, more general types of targets may be expected to encounter specific problems. For example, in our experiments we were relying upon the observers' perceptual experience of the "ideal form," enabling them to detect perceptual distortions. While this could be taken for granted for straight lines or circular forms, it may not apply to other forms, such as conics. The problem could be solved by presenting the "variable" target, superposed with the context pattern, along with a "standard" (non-distorted) form shown side-by-side, and instructing the subject to adjust the variable target to "perceptual equality." Other challenges requiring further mathematical and computational work may occur in determining a suitable base geometry for a given target form. Nonetheless, we believe that the approach proposed in the present paper is a viable one and thus deserves further investigation and testing.

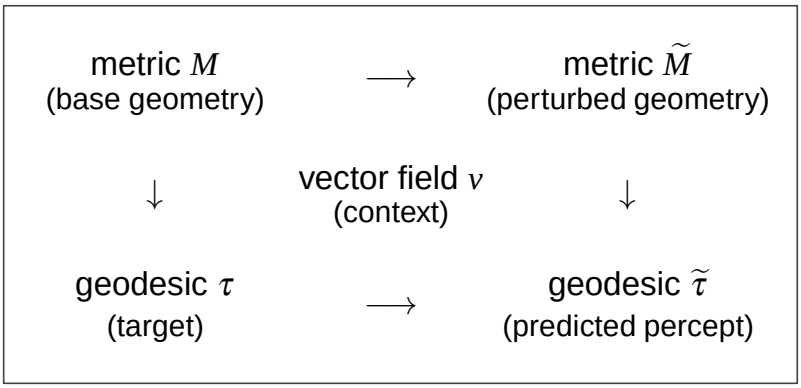

Figure 6. Illustration of the general modeling principle in the form of a commutative diagram.

Acknowledgments

Part of this work was done while the authors were with the Institute for Frontier Areas of Psychology and Mental Health, Freiburg i. Br., Germany. W.E. thanks the Klaus Tschira Foundation for support. We are grateful to Steffen Heinze for his important hint regarding the connection with Riemannian geometry, and Jakob Pacer for assistance in the experiments. Finally, we thank the editor and three anonymous referees for their valuable comments and recommendations.

Appendix

A. Euler–Lagrange equation for the H_α geodesics

The differential equations characterizing geodesic curves commonly are stated using Christoffel symbols derived from the metric tensor (Laugwitz, 1965). A more intelligible, index-free form can be obtained from the Euler–Lagrange equations for the variational problem of minimizing the curve length $L_\alpha(x)$ within the set $\mathcal{X}$ of all twice continuously differentiable curves $t \mapsto x(t)$, $t_0 \le t \le t_1$ in $\mathcal{H}$ with fixed, given endpoints $x(t_0) = \tau_0$, $x(t_1) = \tau_1$. For convenience we shall suppress the parameter t as well as the parameter α wherever possible. Vectors in $\mathbb{R}^2$ are conceived (and treated) as column vectors, but written as row vectors when reference is made to the components. For instance, $\mathfrak{e}_2 = (0, 1)$ is the second basis vector in the standard basis of $\mathbb{R}^2$. The expression $v'(\xi)$ denotes the 2×2 matrix of first-order partial derivatives $\partial v_i(\xi)/\partial \xi_j$ of the vector field $v \equiv v(\xi)$ (Jacobian), and $\omega(\xi) = \partial v_1(\xi)/\partial \xi_2 - \partial v_2(\xi)/\partial \xi_1$ denotes its rotation (evaluated at ξ each). The details of the derivation involve the following steps similar to (Ehm and Wackermann, 2012) (henceforth: EW2012).

STEP 1: *Equivalent minimization problem.* We first consider the more simple problem of minimizing the "energy functional" (cf. Section 4.3)

$$J(x) = \int_{t_0}^{t_1} F(x, \dot{x})\, dt$$

where

$$F(x, \dot{x}) = \langle \dot{x}, H_\alpha(x)\, \dot{x} \rangle = x_2^{-2} \left[|\dot{x}|^2 + 2\alpha \langle \dot{x}, v(x) \rangle^2 \right].$$

A minimizing curve x necessarily satisfies the (vectorial) *Euler–Lagrange equation*

$$\frac{d}{dt} \nabla_{\dot{x}} F(x, \dot{x}) - \nabla_x F(x, \dot{x}) = 0, \tag{6}$$

wherein $\nabla_x F$, $\nabla_{\dot{x}} F$ denote the partial gradients of F with respect to the (vector) arguments x, $\dot{x}$, respectively. For the present F we have

$$\begin{aligned}
\nabla_{\dot{x}} F &= x_2^{-2} \left[2\dot{x} + 4\alpha \langle \dot{x}, v(x) \rangle\, v(x) \right], \\
\frac{d}{dt} \nabla_{\dot{x}} F &= -4\, \frac{\dot{x}_2}{x_2^3} \left[\dot{x} + 2\alpha \langle \dot{x}, v(x) \rangle\, v(x) \right] \\
&\qquad + x_2^{-2} \left[2\ddot{x} + 4\alpha v(x)\, \frac{d}{dt} \langle \dot{x}, v(x) \rangle + 4\alpha \langle \dot{x}, v(x) \rangle\, v'(x)\dot{x} \right], \\
\nabla_x F &= -\frac{2}{x_2^3} \left[|\dot{x}|^2 + 2\alpha \langle \dot{x}, v(x) \rangle^2 \right] + 4\alpha\, \frac{\langle \dot{x}, v(x) \rangle}{x_2^2}\, v'(x)^* \dot{x},
\end{aligned}$$

with $v'(x)^*$ the adjoint of $v'(x)$. With these expressions, the Euler–Lagrange equation becomes

$$\begin{aligned}
0 &= \frac{d}{dt} \nabla_{\dot{x}} F(x, \dot{x}) - \nabla_x F(x, \dot{x}) \\
&= \frac{2}{x_2^2} \left[\ddot{x} + 2\alpha v(x)\, \frac{d}{dt} \langle \dot{x}, v(x) \rangle + 2\alpha \langle \dot{x}, v(x) \rangle\, v'(x)\dot{x} - 2\alpha\, \langle \dot{x}, v(x) \rangle\, v'(x)^* \dot{x} \right] \\
&\qquad - \frac{2}{x_2^3} \left[2\dot{x}_2 \left(\dot{x} + 2\alpha \langle \dot{x}, v(x) \rangle\, v(x) \right) - \left(|\dot{x}|^2 + 2\alpha \langle \dot{x}, v(x) \rangle^2 \right) \mathfrak{e}_2 \right] \\
&= \frac{2}{x_2^2} \left[\ddot{x} + 2\alpha v(x)\, \frac{d}{dt} \langle \dot{x}, v(x) \rangle + 2\alpha \langle \dot{x}, v(x) \rangle \left(v'(x) - v'(x)^* \right) \dot{x} \right] \\
&\qquad - \frac{2}{x_2^3} \left[2\dot{x}_2\, G_\alpha(x)\dot{x} - \langle \dot{x}, G_\alpha(x)\dot{x} \rangle\, \mathfrak{e}_2 \right]
\end{aligned} \tag{7}$$

where $G_\alpha(\xi) = I + 2\alpha v(\xi) \otimes v(\xi)$ as in (4).

We now show that if $t \mapsto x(t)$ is a solution of this equation, then $F(x(t), \dot{x}(t))$ is constant in t. This follows by writing the Euler–Lagrange equation (6) in DuBois–Reymond's form (e. g., (Dacorogna, 2004, Sect. 2.3))

$$\frac{d}{dt}\left(F - \langle \nabla_{\dot{x}} F, \dot{x}\rangle\right)) = \partial_t F$$

and noting that $\partial_t F \equiv 0$ since F does not depend explicitly on t. It follows that

$$\langle \nabla_{\dot{x}} F, \dot{x}\rangle - F = x_2^{-2}\left[2|\dot{x}|^2 + 4\alpha\langle \dot{x}, v(x)\rangle^2\right] - F = 2F - F = F$$

is indeed constant as a function of t. As an easy consequence, a stationary point of the functional $x \mapsto \int_{t_0}^{t_1} F(x, \dot{x})\, dt = J(x)$ is also a stationary point of the functional $x \mapsto \int_{t_0}^{t_1} \sqrt{F(x, \dot{x})}\, dt = L_\alpha(x)$, so in the following we may continue with the former.

Step 2. *Euler–Lagrange equation.* In order to state the Euler–Lagrange equation (7) in explicit form, we use the fact taken from EW2012 that

$$\left(v'(x) - v'(x)^*\right)\dot{x} = \omega|\dot{x}|\rho^\perp$$

where $\rho = \dot{x}/|\dot{x}|$ is the direction of the curve x, $\rho^\perp$ is the unit vector orthogonal to ρ making ρ, $\rho^\perp$ a positively oriented basis of $\mathbb{R}^2$, and $\omega = \partial_1 v_2 - \partial_2 v_1$ is the rotation of the vector field v (evaluated at t and $x(t)$, respectively). Multiplying (7) with $x_2^2/2$ and suppressing the argument $x \equiv x(t)$ of v and G_α gives

$$\begin{aligned}
0 &= \ddot{x} + 2\alpha\, v\, \frac{d}{dt}\langle \dot{x}, v\rangle + 2\alpha\, \langle \dot{x}, v\rangle\, \omega|\dot{x}|\rho^\perp - \frac{1}{x_2}\left[2\dot{x}_2\, G_\alpha \dot{x} - \langle \dot{x}, G_\alpha \dot{x}\rangle\, \mathfrak{e}_2\right] \\
&= \ddot{x} + 2\alpha\, \langle \ddot{x}, v\rangle\, v + 2\alpha\, \langle \dot{x}, v'\dot{x}\rangle\, v + 2\alpha\, \langle \dot{x}, v\rangle\, \omega|\dot{x}|\rho^\perp - \frac{1}{x_2}\left[2\dot{x}_2\, G_\alpha \dot{x} - \langle \dot{x}, G_\alpha \dot{x}\rangle\, \mathfrak{e}_2\right] \\
&= G_\alpha \ddot{x} + 2\alpha\, \langle \dot{x}, v'\dot{x}\rangle\, v + 2\alpha\, \langle \dot{x}, v\rangle\, \omega|\dot{x}|\rho^\perp - \frac{1}{x_2}\left[2\dot{x}_2\, G_\alpha \dot{x} - \langle \dot{x}, G_\alpha \dot{x}\rangle\, \mathfrak{e}_2\right].
\end{aligned}$$

By inversion using $G_\alpha^{-1} = I - \frac{2\alpha}{1+2\alpha}\, v \otimes v$ we obtain

$$\begin{aligned}
\ddot{x} = \frac{2\dot{x}_2}{x_2}\, \dot{x} - \frac{|\dot{x}|^2 + 2\alpha\, \langle \dot{x}, v\rangle^2}{x_2}\left[\mathfrak{e}_2 - \frac{2\alpha v_2}{1+2\alpha}\, v\right] \\
-2\alpha|\dot{x}|^2\left[\frac{\langle \rho, v'\rho\rangle}{1+2\alpha}\, v + \omega\langle \rho, v\rangle\left(\rho^\perp - \frac{2\alpha}{1+2\alpha}\, \langle \rho^\perp, v\rangle\, v\right)\right],
\end{aligned} \tag{8}$$

which is the Euler–Lagrange equation in explicit form.

Step 3: *Reparameterization.* To proceed we switch to the alternative parameterization

$$s = \tanh t, \qquad z(s) = x(\operatorname{arctanh} s).$$

We have $\frac{ds}{dt} = 1 - \tanh^2 t \equiv 1 - s^2$, hence

$$x(t) \equiv z(s), \quad \dot{x}(t) = \frac{dz}{ds}\,\frac{ds}{dt} \equiv z'(s)(1-s^2), \quad \ddot{x}(t) \equiv z''(s)(1-s^2)^2 - 2z'(s)s(1-s^2).$$

Moreover,

$$\frac{\dot{x}(t)}{|\dot{x}(t)|} \equiv \frac{z'(s)}{|z'(s)|} \equiv \rho, \qquad |\dot{x}(t)|^2 \equiv |z'(s)|^2(1-s^2)^2.$$

With these substitutions the Euler–Lagrange equation (8) becomes

$$\begin{aligned}
&(1-s^2)^2\,z'' - 2s(1-s^2)\,z' \\
&= 2\,(1-s^2)^2\,\frac{z_2'}{z_2}\,z' \;-\; (1-s^2)^2\;\frac{|z'|^2 + 2\alpha\langle z', v\rangle^2}{z_2}\left[\mathfrak{e}_2 - \frac{2\alpha v_2}{1+2\alpha}\,v\right] \\
&\quad -2\alpha(1-s^2)^2|z'|^2\left[\frac{\langle \rho, v'\rho\rangle}{1+2\alpha}\,v + \omega\langle\rho, v\rangle\left(\rho^\perp - \frac{2\alpha}{1+2\alpha}\,\langle\rho^\perp, v\rangle\,v\right)\right],
\end{aligned}$$

or after division by $(1-s^2)^2$,

$$\begin{aligned}
z'' \;=\; &2\left(\frac{z_2'}{z_2} + \frac{s}{1-s^2}\right)z' \;-\; \left(1 + 2\alpha\langle\rho, v\rangle^2\right)\frac{|z'|^2}{z_2}\left[\mathfrak{e}_2 - \frac{2\alpha v_2}{1+2\alpha}\,v\right] \\
&-2\alpha\,|z'|^2\left[\frac{\langle\rho, v'\rho\rangle}{1+2\alpha}\,v + \omega\langle\rho, v\rangle\left(\rho^\perp - \frac{2\alpha}{1+2\alpha}\,\langle\rho^\perp, v\rangle\,v\right)\right].
\end{aligned}$$

Regrouping terms according to the vectors involved we obtain the Euler–Lagrange equation in the form used here, stated as Eq. (9) in the following.

Proposition 1. *Consider the variational problem of minimizing the curve length $L_\alpha(z)$ within the set of all twice continuously differentiable curves $s \mapsto z(s)$, $s_0 \le s \le s_1$ in $\mathcal{H}$ with fixed, given endpoints $z(s_0) = \tau_0$, $z(s_1) = \tau_1$. If z is a solution to this problem, it satisfies the (vectorial) Euler–Lagrange equation*

$$\begin{aligned}
z'' \;=\; &2\left(\frac{z_2'}{z_2} + \frac{s}{1-s^2}\right)z' \;-\; \left(1 + 2\alpha\langle\rho, v\rangle^2\right)\frac{|z'|^2}{z_2}\;\mathfrak{e}_2 \;-\; 2\alpha|z'|^2\,\omega\langle\rho, v\rangle\,\rho^\perp \\
&-\frac{2\alpha}{1+2\alpha}\,|z'|^2\left[\langle\rho, v'\rho\rangle - \left(1 + 2\alpha\langle\rho, v\rangle^2\right)\frac{v_2}{z_2} - 2\alpha\omega\langle\rho, v\rangle\langle\rho^\perp, v\rangle\right]v.
\end{aligned} \tag{9}$$

Let us remind here of the tacit understanding that the terms $z, z', z'', \rho, \rho^\perp$ are to be evaluated at the (suppressed) argument s, and v, v', ω at $z(s)$, respectively. The ambiguity in the meaning of the primes in z' and v', which denote differentation w. r. t. the arguments s and ξ, respectively, will not cause confusion.

It is straightforward to check that for $\alpha = 0$, the vertical lines in $\mathcal{H}$ and the half circles orthogonal to the x_1 axis are indeed solutions to (9). In particular, any half circle of the form

$$\tau(s) = r\left(s, \sqrt{1-s^2}\right), \qquad |s| < 1, \tag{10}$$

playing the role of a target stimulus, is a geodesic in the H_0 geometry.

B. Numerical solution

As in EW2012, we use a Picard–Lindelöf type iteration scheme with endpoints fixed at those of the target. Naturally, one would like to have a complete half circle as the target. There are two problems, however. First, the length of a complete half circle is infinite in the given geometry; second, its endpoints are singular points of the differential equation.

Our workaround is as follows. For given radius $r > 0$, pick $s^* \in (0,1)$ close to 1, and take the points $\tau_0^* = \tau(-s^*)$, $\tau_1^* = \tau(s^*)$ on the target (10) as the fixed endpoints for the iterative scheme. In that scheme, a sequence of planar curves $s \mapsto z_n(s)$, approximate solutions to (9) with endpoints at τ_0^*, τ_1^*, is defined as follows: for $|s| \le s^*$ and $n \ge 1$

$$z_0(s) \;=\; \tau(s) \tag{11}$$

$$z_n'(s) \;=\; \int_0^s Q(u, z_{n-1}(u), z_{n-1}'(u))\, du + a_n \tag{12}$$

$$z_n(s) \;=\; \int_0^s z_n'(u)\, du + b_n \tag{13}$$

where $Q(s,z,z')$ is given by the right-hand side of (9) (with s, z, z' substituted by, respectively, u, $z_{n-1}(u)$, $z_{n-1}'(u)$), and the constants a_n, $b_n \in \mathbb{R}^2$ are chosen so that z_n satisfies the boundary conditions:

$$a_n \;=\; \frac{\tau_1^* - \tau_0^* - (\Delta_n^+ - \Delta_n^-)}{2s^*} \tag{14}$$

$$b_n \;=\; \frac{\tau_1^* + \tau_0^* - (\Delta_n^+ + \Delta_n^-)}{2} \tag{15}$$

where

$$\Delta_n^{\pm} = \int_0^{\pm s^*} \int_0^v Q(u, z_{n-1}(u), z_{n-1}'(u))\, du\, dv.$$

Finally, the curves z_n are continued beyond the range $|s| \le s^*$ by setting

$$z_n(s) = \tau(s) \quad \text{for} \quad s^* \le |s| \le 1.$$

Extensive checks showed that this procedure yields numerically robust results eventually independent of the choice of s^* provided s^* is chosen sufficiently close to 1; we

ultimately took $s^* = 1 - 10^{-6}$. Note that if the limit z_∞ of the above scheme exists, it will satisfy Eq. (9), hence represent (for $|s| \le s^*$) a geodesic connecting the points τ_0^*, τ_1^*. The convergence properties of the scheme are briefly discussed in the next appendix. A rigorous convergence proof for an analogous iterative procedure was given in EW2012 for the case of straight line targets.

C. Approximate shape of the perceptual distortion

As anounced in Section 2.3, the exact geodesic γ_α in the perturbed metric H_α will be approximated for small α by a curve of the form $\tau + \alpha\sigma$, where σ depends on the vector field v along τ only. In particular, σ is independent of parameter α, and it represents the *shape* of the perceptual distortion. We derive a differential equation characterizing σ by letting the parameter α tend to zero in (9).

In the following we ignore terms of the order $O(\alpha^2)$. This is indicated by replacing the equality sign by '$\doteq$'. Moreover, the quantities $v, v', \rho, \rho^\perp, \omega$ are understood to be evaluated at $z \equiv \tau(s)$. Making the *ansatz* $z \doteq \tau + \alpha\sigma$ we get for the single components

$$z_1 \doteq rs + \alpha\sigma_1, \quad z_1' \doteq r + \alpha\sigma_1', \quad z_1'' \doteq \alpha\sigma_1'',$$

$$z_2 \doteq r\sqrt{1-s^2} + \alpha\sigma_2, \quad z_2' \doteq -\frac{rs}{\sqrt{1-s^2}} + \alpha\sigma_2', \quad z_2'' \doteq -\frac{r}{(1-s^2)^{3/2}} + \alpha\sigma_2''.$$

Therefore,

$$\begin{aligned}\frac{z_2'}{z_2} &\doteq \frac{-\frac{rs}{\sqrt{1-s^2}} + \alpha\,\sigma_2'}{r\sqrt{1-s^2}\left(1 + \frac{\alpha\,\sigma_2}{r\sqrt{1-s^2}}\right)} \doteq -\frac{s}{1-s^2} + \frac{\alpha\,\sigma_2'}{r\sqrt{1-s^2}} + \frac{\alpha\,s\,\sigma_2}{r(1-s^2)^{3/2}} \\ &= -\frac{s}{1-s^2} + \frac{\alpha}{r\sqrt{1-s^2}}\left(\sigma_2' + \frac{s}{1-s^2}\,\sigma_2\right),\end{aligned}$$

and similarly

$$\begin{aligned}|z'|^2 &\doteq \frac{r^2}{1-s^2} + 2\alpha\,r\left(\sigma_1' - \frac{s}{\sqrt{1-s^2}}\,\sigma_2'\right), \\ \frac{|z'|^2}{z_2} &\doteq \frac{r}{(1-s^2)^{3/2}} + 2\alpha\left(\frac{\sigma_1'}{\sqrt{1-s^2}} - \frac{s}{1-s^2}\,\sigma_2' - \frac{\sigma_2}{2(1-s^2)^2}\right).\end{aligned}$$

Inserting these expressions into the Euler–Lagrange equation (9) we obtain for the first and second components

$$\alpha\sigma_1'' \doteq \frac{2\alpha}{r\sqrt{1-s^2}}\left[\sigma_2' + \frac{s}{1-s^2}\,\sigma_2'\right](r + \alpha\sigma_1') - \frac{2\alpha\,r^2}{1-s^2}\left[\left(\langle\rho, v'\rho\rangle - \frac{v_2}{\tau_2}\right)v_1 + \omega\langle\rho, v\rangle\,\rho_1^\perp\right]$$

and

$$-\frac{r}{(1-s^2)^{3/2}} + \alpha\sigma_2'' \doteq \frac{2\alpha}{r\sqrt{1-s^2}}\left[\sigma_2' + \frac{s}{1-s^2}\,\sigma_2'\right]\frac{-rs}{\sqrt{1-s^2}} - \frac{r}{(1-s^2)^{3/2}}$$
$$-2\alpha\left(\frac{\sigma_1'}{\sqrt{1-s^2}} - \frac{s}{1-s^2}\,\sigma_2' - \frac{\sigma_2}{2(1-s^2)^2}\right) - \frac{2\alpha\, r\,\langle\rho, v\rangle^2}{(1-s^2)^{3/2}}$$
$$-\frac{2\alpha\, r^2}{1-s^2}\left[\left(\langle\rho, v'\rho\rangle - \frac{v_2}{\tau_2}\right)v_2 + \omega\langle\rho, v\rangle\,\rho_2^{\perp}\right],$$

respectively. Regrouping terms, dividing by α, then ignoring terms of order $O(\alpha)$ gives the following.

Proposition 2. *The shape $\sigma = (\sigma_1, \sigma_2)$ of the perceptual distortion satisfies the following system of differential equations,*

$$\sigma_1'' = \frac{2}{1-s^2}\left[\sqrt{1-s^2}\,\sigma_2' + \frac{s}{\sqrt{1-s^2}}\,\sigma_2 - r^2 v_1\left(\langle\rho, v'\rho\rangle - \frac{v_2}{\tau_2}\right) - r^2\omega\langle\rho, v\rangle\,\rho_1^{\perp}\right], \quad (16)$$

$$\sigma_2'' = -\frac{2}{1-s^2}\left[\sqrt{1-s^2}\,\sigma_1' + \frac{s^2-1/2}{1-s^2}\,\sigma_2 + \frac{r\langle\rho, v\rangle^2}{\sqrt{1-s^2}}\right. \quad (17)$$
$$\left. + r^2 v_2\left(\langle\rho, v'\rho\rangle - \frac{v_2}{\tau_2}\right) + r^2\omega\langle\rho, v\rangle\,\rho_2^{\perp}\right].$$

We remind here of our stipulation that v, e.g., is evaluated at $z(s) = \tau(s)$, and likewise for the other quantities, $v', \rho, \rho^{\perp}, \omega$. Thus all terms besides σ and its derivatives are known once the vector field v and the target τ (i.e., the radius r) are fixed, meaning that the shape can indeed be derived from the system (16), (17). In the case of a straight line target treated in EW2012, this calculation reduced to just (twofold) integration. Here we have to solve a proper differential equation (system) which is, again, accomplished by Picard–Lindelöf iteration as described in the previous appendix, setting σ and σ' identically 0 in the beginning.

These algorithms for solving the equations in Propositions 1 and 2 converged for all contexts considered in our study, uniformly in the range $|\alpha| \le 0.1$ (which is sufficiently large since all α estimates in the experiment were $\le .07$). Convergence was not as rapid as for straight line targets, yet stationarity virtually was reached after 11 iterations. We therefore took the $N = 11$-th iterates $z_N \equiv z_{\alpha,N}$ and σ_N of the respective Picard–Lindelöf schemes as substitutes for the exact geodesic γ_α and shape σ. Finally, discrepancies between the curves $z_{\alpha,N}$ and $\widetilde{z}_{\alpha,N} = \tau + \alpha\sigma_N$ were minimal to indiscernible by eye in all cases.

D. Special case of a context consisting of horizontal lines

Explicit solutions to (16), (17) generally are not available. An interesting exception is the case of a context consisting of horizontal lines. Then $v_1 \equiv 1$, $v_2 \equiv 0$, say, and

$v' \equiv 0$, $\omega \equiv 0$. Since the components of ρ evaluated along τ are $\rho_1 = \sqrt{1-s^2}$, $\rho_2 = -s$, the system (16), (17) reduces to

$$\sigma_1'' = \frac{2}{1-s^2}\left[\sqrt{1-s^2}\,\sigma_2' + \frac{s}{\sqrt{1-s^2}}\,\sigma_2\right], \tag{18}$$

$$\sigma_2'' = -\frac{2}{1-s^2}\left[\sqrt{1-s^2}\,\sigma_1' + \frac{s^2-1/2}{1-s^2}\,\sigma_2 + r\sqrt{1-s^2}\right]. \tag{19}$$

To study this case it is convenient to assume that the shape σ is of the form $\sigma = \tau\,\widetilde{\sigma}$ (coordinatewise multiplication), so that in view of $z \doteq \tau(1+\alpha\,\widetilde{\sigma})$ the curve $\widetilde{\sigma}$ represents a kind of multiplicative shape. With this substitution the system (18), (19) becomes

$$\widetilde{\sigma}_1'' = \frac{2}{s}\left(\widetilde{\sigma}_2' - \widetilde{\sigma}_1'\right), \tag{20}$$

$$\widetilde{\sigma}_2'' = \frac{2}{1-s^2}\left(\widetilde{\sigma}_2 - \widetilde{\sigma}_1 - 1 + s(\widetilde{\sigma}_2' - \widetilde{\sigma}_1')\right). \tag{21}$$

Now, subtracting (20) from (21) and putting $\eta = \widetilde{\sigma}_2 - \widetilde{\sigma}_1 - 1$ we get the single differential equation

$$\eta'' = \frac{2}{s(1-s^2)}\left(s\eta + (2s^2-1)\eta'\right),$$

the general solution of which is $\eta = A\lambda + B/s$ where

$$\lambda(s) = \frac{1}{s}\,\log\frac{1+s}{1-s}, \tag{22}$$

and A, B are constants. Clearly $B = 0$, since otherwise one would have a pole at $s = 0$. Direct integration of (20) gives at first

$$\widetilde{\sigma}_1'(s) = \int_0^s \frac{2\eta'(u)}{u}\,du + C = A\,\frac{(1+s^2)\,\lambda(s) - 2}{s} + C,$$

then

$$\widetilde{\sigma}_1 = A\left(2 - (1-s^2)\,\lambda\right) + Cs + D,$$

and thus

$$\widetilde{\sigma}_2 = \eta + \widetilde{\sigma}_1 + 1 = A\left(s^2\,\lambda + 2\right) + Cs + D + 1.$$

The constants C, D can be determined from the condition that $\sigma_1(s) = rs\widetilde{\sigma}_1(s)$, and hence $\widetilde{\sigma}_1(s)$, has to vanish at $s = \pm 1$. Thus $2A - C + D = 0$, $2A + C + D = 0$, and so $C = 0$, $D = -2A$. Perhaps surprisingly, there appears to be no condition fixing the value of A. Note that the condition $\sigma_2(s) = r\sqrt{1-s^2}\,\widetilde{\sigma}_2(s) = 0$ at $s = \pm 1$ does not help since the factor $\sqrt{1-s^2}$ vanishes there.

Summarizing, we have determined the shape σ of the perceptual distortion in the case of a horizontal lines context up to a constant $A > 0$: its components are

$$\sigma_1(s) = rsA(s^2-1)\lambda(s), \quad \sigma_2(s) = r\sqrt{1-s^2}\left(1 + As^2\lambda(s)\right), \tag{23}$$

where λ is defined by (22). It should be noted that the resulting prediction $z^*_{\alpha,A} = \tau + \alpha\sigma$ (with $\sigma \equiv \sigma_A$ from (23)) for the distorted percept is not just an ellipse. Remarkably also, the curves $z^*_{\alpha,A}$ are for $A = 1, 1/8, 1/32$ virtually indistinguishable from each other, and also from the approximations $z_{\alpha,N}$ and $\widetilde{z}_{\alpha,N}$ considered in Appendix C.

E. Contexts used in the experiment

A context consists of a finite sample from a family of curves $u \mapsto C_\theta(u)$ depending on a real parameter θ. We specifically consider curves of the form $C_\theta(u) = (u, \theta q(u))$, where q is a smooth function positive on a domain enclosing the domain covered by the target. The components of the associated (normalized) vector field $v = (v_1, v_2)$ then are

$$v_1(\xi) = \frac{1}{\sqrt{1 + \xi_2^2\,[\frac{q'}{q}(\xi_1)]^2}}, \qquad v_2(\xi) = \frac{\xi_2\,\frac{q'}{q}(\xi_1)}{\sqrt{1 + \xi_2^2\,[\frac{q'}{q}(\xi_1)]^2}},$$

and the Jacobian of v is

$$v'(\xi) = \left(1 + \left(\xi_2\,\frac{q'}{q}\right)^2\right)^{-3/2} \begin{pmatrix} -\xi_2^2\,\frac{q'}{q}\left(\frac{q'}{q}\right)' & -\xi_2\left(\frac{q'}{q}\right)^2 \\ \xi_2\left(\frac{q'}{q}\right)' & \frac{q'}{q} \end{pmatrix},$$

with q, q', q'' evaluated at ξ_1. Note that if θ varies in an interval of the form $[-b, b]$ $(b > 0)$, the context curves lie symmetrically about the x_1 axis; they are symmetrical w. r. t. the x_2 axis if q is an even function. The four contexts C1 to C4 used in the experiment were specified by the functions $q \equiv \{q(u),\ |u| \le 2r\}$ given in the following table; r is the radius of the respective target circle. The resulting figures were scaled such that the target circles had diameter 9 cm in the physical stimuli presented to the observers.

context	function $q(u)$	radius r
C1	$1 + u^2$	0.5
C2	$1 + 1/\sqrt{1+u^2}$	2.0
C3	$(u+3)^2$	1.0
C4	1	1.0

Supplementary material about experimental details is available from the authors upon request.

References

Avery, G. C. & Day, R. H. (1969). Basis of the horizontal-vertical illusion. *Journal of Experimental Psychology*, *81*, 376–380.

Blumenfeld, W. (1913). Untersuchungen über die scheinbare Grösse im Sehraume. *Zeitschrift für Psychologie und Physiologie der Sinnesorgane*, *65*, 241–404.

Boring, E. G. (1942). *Sensation and perception in the history of experimental psychology*. New York: Appleton.

Burns, B. D. & Pritchard, R. (1971). Geometrical illusions and the response of neurones in the cat's visual cortex to angle patterns. *Journal of Physiology*, *213*, 599–616.

Cannon, J. W., Floyd, W. J., Kenyon, R., & Parry, W. R. (1997). Hyperbolic Geometry. In: *Flavors of Geometry*, MSRI Publ., 1997, pp. 59–115.

Carpenter, R. H. S. & Blakemore, C. (1973). Interactions between orientations in human vision. *Experimental Brain Research*, *18*, 287–303.

Changizi, M. A., Hsieh, A., Nijhawan, R., Kanai, R., & Shimojo, S. (2008). Perceiving the present and a systematization of illusions. *Cognitive Science*, *32*, 459–503.

Coren, S., Girgus, J. S., Erlichman, H., & Hakstian, A. R. (1976). An empirical taxonomy of visual illusions. *Perception & Psychophysics*, *20*, 129–137.

Coren, S. & Girgus, J. S. (1978). *Seeing is deceiving: The psychology of visual illusions*. Lawrence Erlbaum: Hillsdale (NJ).

Dacorogna, B. (2004). *Introduction to the calculus of variations*. London: Imperial College Press.

Eagleman, D. M. (2001). Visual illusions and neurobiology. *Nature Reviews Neuroscience*, *2*, 920–926.

Ehm, W. & Wackermann, J. (2012). Modeling geometric–optical illusions: A variational approach. *Journal of Mathematical Psychology*, *56*, 404–416.

Ehm, W. & Wackermann, J. (2013). Hyperbolic geometry of Ehrenstein–Orbison type illusions. In J. Wackermann, M. Wittmann, & W. Skrandies (Eds.), *Fechner Day 2013* (p. 49). Freiburg, Germany: International Society for Psychophysics.

Ehrenstein, W. (1925). Versuche über die Beziehungen zwischen Bewegungs- und Gestaltwahrnehmung. *Zeitschrift für Psychologie*, *96*, 305–352.

Fermüller, C. & Malm, H. (2004). Uncertainty in visual processes predicts geometrical optical illusions. *Vision Research*, *44*, 727–749.

French, R. (1987). The geometry of visual space. *Noûs*, *21*, 115–133.

Gori, S. & Stubbs, D. A. (2014). Motion illusions as a psychophysical tool to investigate the visual system. In Geremek, A., Greenlee, M. W., & Magnussen, S. (Eds.), *Perception beyond Gestalt: Progress in vision research* (pp. 128–143). New York, U.S.A.: Psychology Press.

Gregory, R. L. (1963). Distortion of visual space as inappropriate constancy scaling. *Nature*, *199*, 678–680.

Gregory, R. L. (1997). Knowledge in perception and illusion. *Phil. Trans. R. Soc. Lond. B*, *352*, 1121–1128.

Gregory, R. L. (1997). Visual illusions classified. *Trends in Cognitive Sciences*, *1*, 190–194.

Hatfield, G. & Epstein, W. (1985). The status of the minimum principle in the theoretical analysis of visual perception. *Psychological Bulletin*, *97*, 155–186.

Heelan, P. A. (1983). *Space perception and philosophy of science*. Berkeley: University of California Press.

Helmholtz, H. (1867). *Handbuch der physiologischen Optik* (3 vols.). Leipzig: Voss.

Hering, E. (1861). *Beiträge zur Physiologie I. Vom Ortsinne der Netzhaut*. Leipzig: Engelmann.

Hoffman, W. C. (1966). The Lie algebra of visual perception. *Journal of Mathematical Psychology*, *3*, 65–98.

Hoffman, W. C. (1971). Visual illusions of angle as an application of Lie transformation groups. *SIAM Review*, *13*, 169–184.

Horrell, R. I. (1971). The angle of intersection of contours as the determinant of a geometric illusion. *Perception & Psychophysics*, *10*, 208–210.

Hotopf, W. H. N. & Ollerearnshaw, C. (1972). The regression to right angles tendency and the Poggendorf illusion I, II. *British Journal of Psychology*, *63*, 359–367 and 369–379.

Hotopf, W. H. N. & Robertson, S. H. (1975). The regression to right angles tendency, lateral inhibition, and the transversals in the Zöllner and Poggendorf illusions. *Perception & Psychophysics*, *18*, 453–459.

Indow, T. (1991). A critical review of Luneburg's model with regard to global structure of visual space. *Psychological Review*, *98*, 430–453.

Kundt, A. (1863). Untersuchungen über Augenmaass und optische Täuschungen. *Annalen der Physik und Chemie*, *196*, 118–158.

Laugwitz, D. (1965). *Differential and Riemannian geometry*. New York: Academic Press.

Lehmann, G. (1967). Die Analyse geometrisch-optischer Täuschungen durch Vektorfelder. *Zeitschrift für Experimentelle und Angewandte Psychologie*, *14*, 442–462.

Livingstone, M. S. & Hubel, D. H. (1987). Psychophysical evidence for separate channels for the perception of form, color, movement, and depth. *Journal of Neuroscience*, *7*, 3416–3468.

Luneburg, R. K. (1948). *Mathematical analysis of binocular vision*. Princeton: Princeton University Press.

Luneburg, R. K. (1950). The metric of visual space. *Journal of the Optical Society of America*, *40*, 627–642.

Mach, E. (1866). Über die physiologische Wirkung räumlich vertheilter Lichtreize, 3. Abhandlung. *Sitzungsberichte der mathematisch-naturwissenschaftlichen Classe der Kaiserlichen Akademie der Wissenschaften, Wien*, *54/2*, 393–408.

Mach, E. (1868). Über die physiologische Wirkung räumlich vertheilter Lichtreize, 4. Abhandlung. *Sitzungsberichte der mathematisch-naturwissenschaftlichen Classe der Kaiserlichen Akademie der Wissenschaften, Wien*, *57/2*, 11–19.

Maniatis, L. M. (2015). First, believe your eyes. *Perception*, *44*, 1149–1152.

Metzger, W. (1975). *Gesetze des Sehens* (3rd ed.). Frankfurt: Kramer.

Müller-Lyer, F. C. (1889). Optische Urteilstäuschungen. *Archiv für Anatomie und Physiologie, Physiologische Abteilung 2 (Supplement)*, *9*, 263–270.

Oppel, J. J. (1855). Über geometrisch-optische Täuschungen. *Jahresbericht des physikalischen Vereins zu Frankfurt am Main*, *1854/55*, 37–47.

Oppel, J. J. (1861). Über geometrisch-optische Täuschungen (Zweite Nachlese). *Jahresbericht des physikalischen Vereins zu Frankfurt am Main*, *1860/61*, 26–37.

Orbison, W. D. (1939). Shape as a function of the vector-field. *American Journal of Psychology*,

52, 31–45.

Robinson, J. O. (1998). *The psychology of visual illusion* (2nd ed.). Mineola (NY): Dover.

Rock, I. In defense of unconscious inference. In: Epstein, W. (ed.), *Stability and constancy in visual perception: Mechanisms and processes* (pp. 321–373), New York: Wiley, 1977.

Rogers, B. (2014). Delusions about illusions. *Perception*, *43*, 840–845.

Smith, D. A. (1978). A descriptive model for perception of optical illusions. *Journal of Mathematical Psychology*, *17*, 64–85.

Suppes, P. (1977). Is visual space Euclidean? *Synthese*, *35*, 397–421.

Thompson, P. & Mikellidou, K. (2011). Applying the Helmholtz illusion to fashion: Horizontal stripes won't make you look fatter. *i-Perception*, *2*, 69–76.

Turner, R. S. (1994). *In the eye's mind*. Princeton: Princeton University Press.

Wackermann, J. (2010). Geometric–optical illusions: A pedestrian's view of the phenomenal landscape. In A. Bastianelli & G. Vidotto (Eds.), *Fechner Day 2010* (pp. 171–176). Padova, Italy: International Society for Psychophysics.

Wackermann, J. (2011a). Geometry of visual space: What's in a name? In D. Algom et al. (Eds.), *Fechner Day 2013* (pp. 25–30). Ra'anana, Israel: International Society for Psychophysics.

Wackermann, J. (2011b). Filled space expansion: Constants, variants and determinants of the Oppel–Kundt phenomenon. In D. Algom et al. (Eds.), *Fechner Day 2011* (pp. 47–52). Ra'anana, Israel: International Society for Psychophysics.

Wagner, M. (1985). The metric of visual space. *Perception and Psychophysics*, *38*, 483–495.

Wagner, M. (2006). *The geometries of visual space*. Mahwah: Lawrence Erlbaum.

Walker, E. H. (1973). A mathematical theory of optical illusions and figural aftereffects. *Perception & Psychophysics*, *13*, 467–486.

Westheimer, G. (2008). Illusions in the spatial sense of the eye: Geometrical–optical illusions and the neural representation of space. *Vision Research*, *48*, 2128–2142.

Wolfe, U., Maloney, L. T., & Tam, M. (2005). Distortions of perceived length in the frontoparallel plane: Tests of perspective theories. *Perception & Psychophysics*, *67*, 969–979.

Yazdanbakhsh, A. & Gori, S. (2011). Mathematical analysis of the Accordion Grating illusion: A differential geometry approach to introduce the 3D aperture problem. *Neural Networks*, *24*, 1093–1101.

Zavagno, D., Daneyko, O., & Actis-Grosso, R. (2015). Mishaps, errors, and cognitive experiences: on the conceptualization of perceptual illusions. *Frontiers in Human Neuroscience*, *9*, 190.

Zhang, J. & Wu, S. (1990). Structure of visual perception. *Proceedings of the National Academy of Sciences USA*, *87*, 7819–7823.

Zöllner, F. (1860). Ueber eine neue Art von Pseudoskopie und ihre Beziehungen zu den von Plateau und Oppel beschriebenen Bewegungsphänomenen. *Annalen der Physik und Chemie*, *186*, 500–523.

Zöllner, J. C. F. (1872). *Über die Natur der Cometen. Geschichte und Theorie der Erkenntniss* (2nd ed.). Leipzig: Engelmann.